Strategies to increase the quantum yield: Luminescent methoxylated imidazo[1,5-a]pyridines

Giorgio Volpi, Claudio Garino, Elisa Fresta, Enrico Casamassa, Marco Giordano, Claudia Barolo, Guido Viscardi.

Strategies to increase the quantum yield: luminescent methoxylated imidazo[1,5-*a*]pyridines

Dyes and Pigments, 192509, 2021, 109463.

DOI: 10.1016/j.dyepig.2021.109455

Strategies to increase the quantum yield: luminescent methoxylated imidazo[1,5-*a*]pyridines

G. Volpi,[a] C. Garino,[a] E. Fresta,[b] E. Casamassa,[c d] M. Giordano,[a] C. Barolo,[a e] G. Viscardi[a]

[a] Department of Chemistry, NIS Interdepartmental Centre and INSTM Reference Centre, University of Turin, Via P. Giuria 7, 10125, Torino, Italy
[b] Chair of Biogenic Functional Materials, Technical University of Munich, Schulgasse 22 D-94315, Straubing, Germany
[c] Centre of Advanced Innovation Technologies, VSB – Technical University of Ostrava, Ostrava, 708 33, Czech Republic
[d] Italian National Research Council, ICMATE, Via de Marini 6, 16149, Genova, Italy
[e] ICxT Interdepartmental Centre, University of Turin, Lungo Dora Siena 100, 10153 Torino, Italy

Keywords: imidazo[1,5-*a*]pyridine, luminescence, fluorescence, large Stokes shift, down shifting, methoxylated

Abstract

A series of methoxylated imidazo[1,5-*a*]pyridines is presented and their optical and electrochemical properties investigated and interpreted on the basis of density functional theory calculations. The photophysical properties are discussed in relation to the chemical structure. The key role of the 1,3 substitutions on the imidazo[1,5-*a*]pyridine nucleus on rotational barriers and on frontier molecular orbitals is discussed in relation to the experimental hyperchromic effect, photoemission quantum yield and electrochemical properties. Depending on the position of the introduced methoxy substituents on the imidazo[1,5-*a*]pyridine nucleus, we are able to tune the Stokes shift and to increase the emission quantum yield from 22% to 50%.

1. Introduction

Luminescent and electroluminescent small organic molecules are widely employed in everyday products, like digital displays of televisions, smartphones and wearable devices.[1–3] Defined emission properties, in a selected spectral region, such as high quantum yield and intense absorption, optical tunability and large Stokes shift (to avoid reabsorption) are essential requirements for any fluorophore designed for fluorescence microscopy, down-converting technologies, lighting devices or any other field in which luminescent molecules are employed.[4–8]

In this context, imidazo[1,5-*a*]pyridine derivatives are receiving an increasing interest[9] for several applications in materials science,[10] nonlinear optics (NLO),[11] confocal microscopy,[12,13] fluorescence sensing,[14–16] and for pharmaceutical and medical research.[17–20] Meanwhile, the electroluminescence of imidazo[1,5-*a*]pyridines has been recently investigated for the first time by G. Albrecht *et al.*, employing layered OLEDs based on this fluorogenic nucleus as emitting system.[21,22] Regarding the use of coordination compounds containing imidazo[1,5-*a*]pyridine derivatives, up to now only copper complexes bearing imidazo[1,5-*a*]pyridine ligands have been employed in light emitting electrochemical cells.[23,24]

Among the different families of luminophores, the imidazo[1,5-*a*]pyridine core is widely studied owing to: i) intense blue emission with large Stokes shift, ii) good optical tunability, and iii) moderate photoluminescence quantum yields (ϕ).[11,14,25–27] Furthermore, using appropriate substitution patterns, coordination metal complexes can be obtained and, in general, the modification of the imidazo[1,5-*a*]pyridine nucleus by coordinating substituents can lead to substantial modifications of the optical behaviour.[28–31]

In a few previous works, differently substituted imidazo[1,5-*a*]pyridines were synthetized and characterized to find a relationship between optical properties and chemical modifications in position 1 of the imidazo[1,5-*a*]pyridine skeleton. As clearly reported in these papers,[32–35] the methoxy group is regarded as the best substituent to increase the emissive behaviour of the imidazo[1,5-*a*]pyridine nucleus. For such reason, herein, we present a systematic study on the synthesis and optical characterization of differently methoxylated imidazo[1,5-*a*]pyridine derivatives (Figure 1). The fluorophores have been designed to investigate the relationship between the chemical structure (i.e. the position and the number of the conjugated methoxy groups on the dye skeleton) and the electronic behaviour, in order to further optimize the optical properties and pave the way, also for this class of simple and low cost emitters, to a real application in sensors, in fluorescence microscopy imaging or even in energy related devices (from lighting to photovoltaic applications).

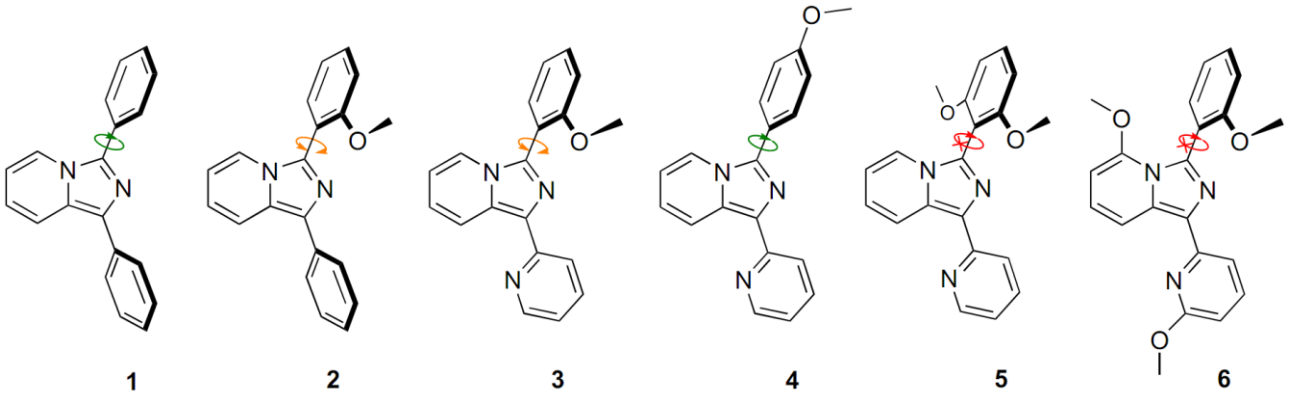

Figure 1. Chemical structures of the studied 1,3-substituted-imidazo[1,5-*a*]pyridines.

2. Results and discussion

2.1. Synthesis

Compounds **1**–**6** are based on the luminescent imidazo[1,5-*a*]pyridine skeleton and were obtained applying previously reported synthetic approaches. In particular, compounds **1** and **2** were prepared by condensation of phenyl(pyridin-2-yl)methanone with benzaldehyde or 2-methoxybenzaldehyde, respectively;[32,34,36] compounds **3–5** were synthesised through the condensation of di(2-pyridyl)ketone with different aldehydes: 2-methoxybenzaldehyde for compound **3**, 4-methoxybenzaldehyde for **4** and 2,6-dimethoxybenzaldehyde for compound **5**;[19,24,37] compound **6** was prepared by condensation of bis(6-methoxypyridin-2-yl)methanone with 2-methoxybenzaldehyde. Compounds **5** and **6** are new molecules and have never been reported before. Compound **1** can be considered a well-known reference for fluorescent imidazo[1,5-*a*]pyridine; without chemical groups on the aromatic substituents in position 1 and 3. Compound **2** was chosen as a starting point owing to its excellent emission properties, as highlighted in previous works focused on the photophysical properties of different 3-substituted-imidazo[1,5-*a*]pyridine dyes.[31,35,38,39] In particular, **2** displays the highest ϕ if compared to similar 1,3-substituted-imidazo[1,5-*a*]pyridine derivatives. Since compound **2** shows a methoxy group, we decided to investigate the effect of this specific substituent in different positions.

To further improve the emissive features of **2**, we adopted two different structural strategies: i) the substitution of the phenyl group in position 1 with a pyridine group, and ii) the introduction of methoxy groups in four different positions (Figure 1). The effects of these structural and electronical modifications on the emission properties of the studied fluorophores are herein discussed.

2.2 Characterization

The absorption and emission spectra of **1**–**6** are shown in Figure 2 and 7 and selected photophysical data are reported in Table 1.

All the compounds are characterized by two main bands peaking at λ_{max} ~ 300 nm and λ_{max} 360–380 nm, with almost no absorption beyond 430 nm. **1**–**5** show a higher molar absorbance value for the first peak (300–320 nm) if compared to the second one (340–370). Overall, all the molecules have a good log(**ε**) value of ~4. Furthermore, the intensity of the lowest-energy band significantly increases going from compounds **1** and **2** to **3**–**6**. Such hyperchromic effect, induced by the substitution of the phenyl group (**1** and **2**) with the pyridine (**3**–**6**) in position 1 on the imidazo[1,5-*a*]pyridine nucleus, is predicted by TDDFT calculations: upon introduction of a pyridyl moiety, the oscillator strength of the first electronic transition significantly increases (Figures 3). This behaviour can be rationalized considering the molecular conformation in the ground state calculated by DFT and the corresponding frontier orbitals (Figure 4). Indeed, the nitrogen atom of pyridine derivatives **3**–**6** leads to a planarization of this peripheral moiety with the imidazo[1,5-*a*]pyridine core, due to i) the missing repulsion of the hydrogen atom previously bound to the replaced carbon in **1** and **2**, and ii) to the interaction between the lone pair of nitrogen and the neighbouring hydrogen atom at the core.[40]

The lowest-energy singlet electronic transition can be considered a π-π^*, essentially involving the highest-occupied molecular orbital (HOMO) and the lowest unoccupied molecular orbital (LUMO), for all the considered compounds (see Tables S1–S6 in the supplementary data section, for details). The HOMO is spread over the imidazo[1,5-*a*]pyridine nucleus and the aromatic substituent in position 1, whereas the LUMO is located mainly on the imidazo[1,5-*a*]pyridine nucleus of **1** and **2**,

in which the phenyl group is twisted out of the imidazo[1,5-*a*]pyridine plane, and for **3**–**6** it also extends over the pyridyl moiety, as a consequence of the structural planarization. In other words, the planarization directly affects the magnitude of the transition dipole by increasing the overlap of the wave functions.[35]

The introduction of the methoxy group in different positions of the 1,3-substituted-imidazo[1,5-*a*]pyridine (**2**–**6**) does not cause a strong shift in the absorbance maxima in comparison to compound **1** (see Table 1). This behaviour is confirmed by TDDFT calculations, as evident by the computed singlet excited state transitions reported in Figure 3. More in details, observing the EDDM (Electron Density Difference Map) relative to transition 1 (Figures 3), it is evident how the phenyl or the pyridine substituent in position 1 are involved in the electronic transition with an opposite effect. Indeed, the substitution results in a blue-shift of the low energy transition of compounds containing the pyridine (**3**–**6**), compared to those bearing the phenyl (**1**, **2**). TDDFT calculations also point out the limited involvement of the methoxy groups in the first electronic transition.

Table 1. Selected photophysical properties of compound **1**–**6** in dichloromethane solution (10^{-5} M).

Compound	λ_{abs} (nm)	λ_{em} (nm)	Stokes shift (nm)	Log(ε) ($M^{-1}cm^{-1}$)	ϕ
1	306 342 sh	481	175	4.30 4.09	0.22
2	301 374 sh	474	173	4.36 3.86	0.38
3	320 370	457	87	4.07 4.06	0.36
4	320 375	469	94	4.25 3.88	0.24
5	330 367	455	88	4.11 3.98	0.50
6	375 400 sh	413 sh 433 460 sh	58	4.11	0.36

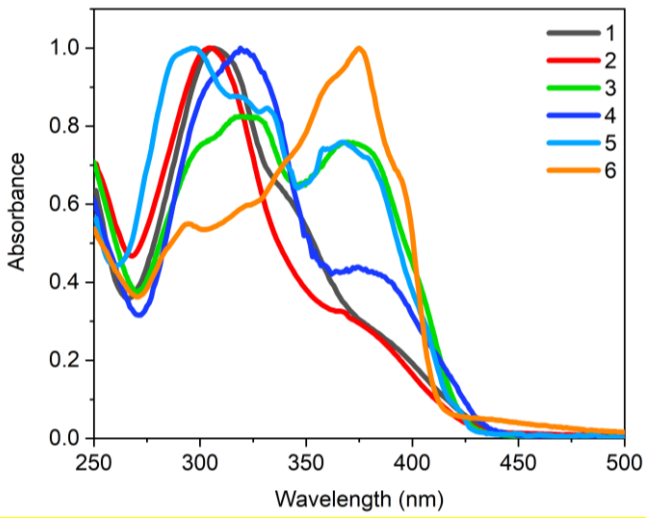

Figure 2. Normalized absorption spectra of **1**–**6** in dichloromethane solution (10^{-5} M).

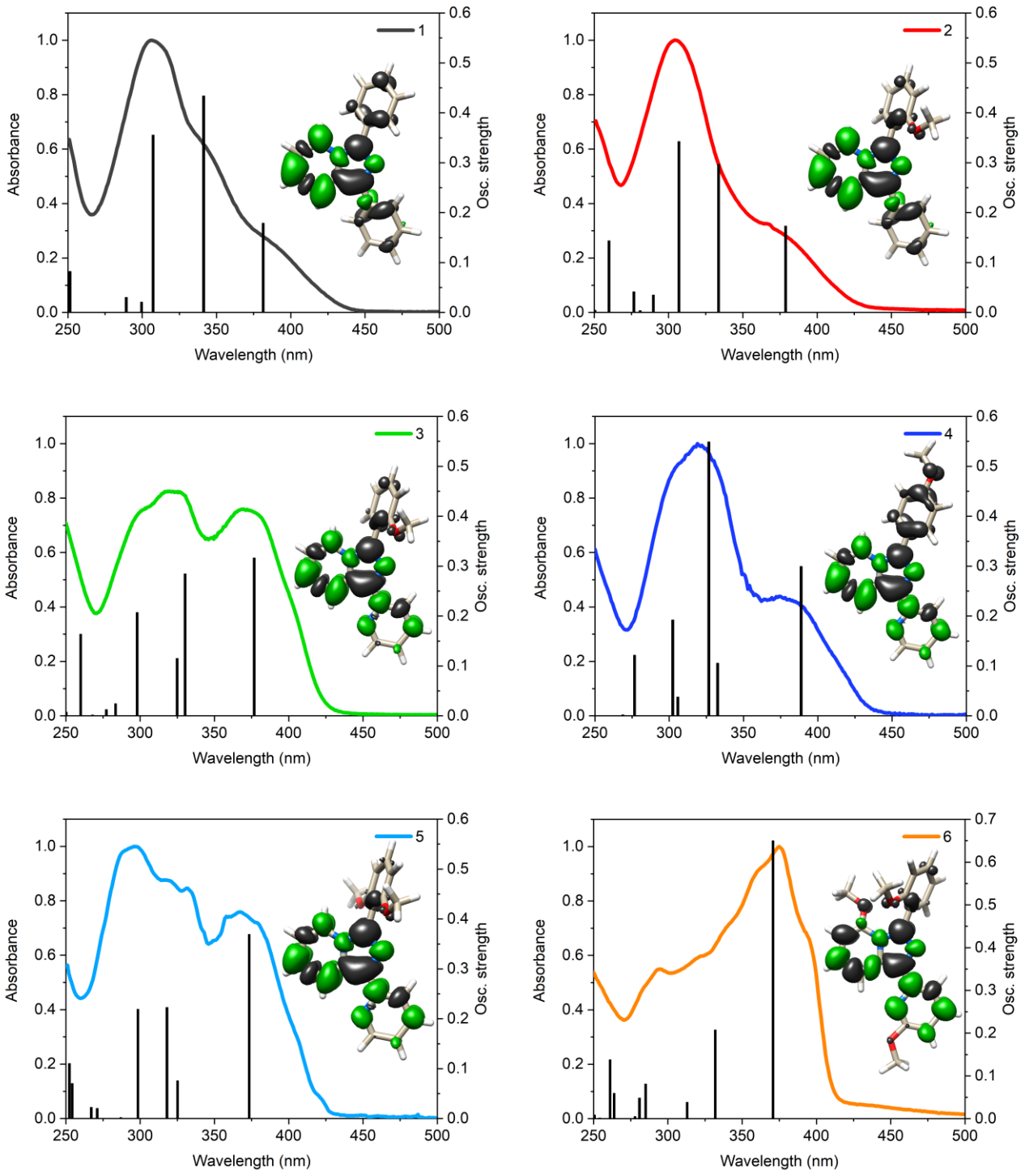

Figure 3. Experimental electronic absorption spectra of **1**–**6** in dichloromethane solution (10^{-5} M) together with calculated singlet excited state transitions computed from the ground state, as vertical excitation with linear response solvation (vertical bars with height equal to the oscillator strength values). EDDM for the lowest energy singlet electronic transition computed by TDDFT (black indicates a decrease in electron density while green indicates an increase).

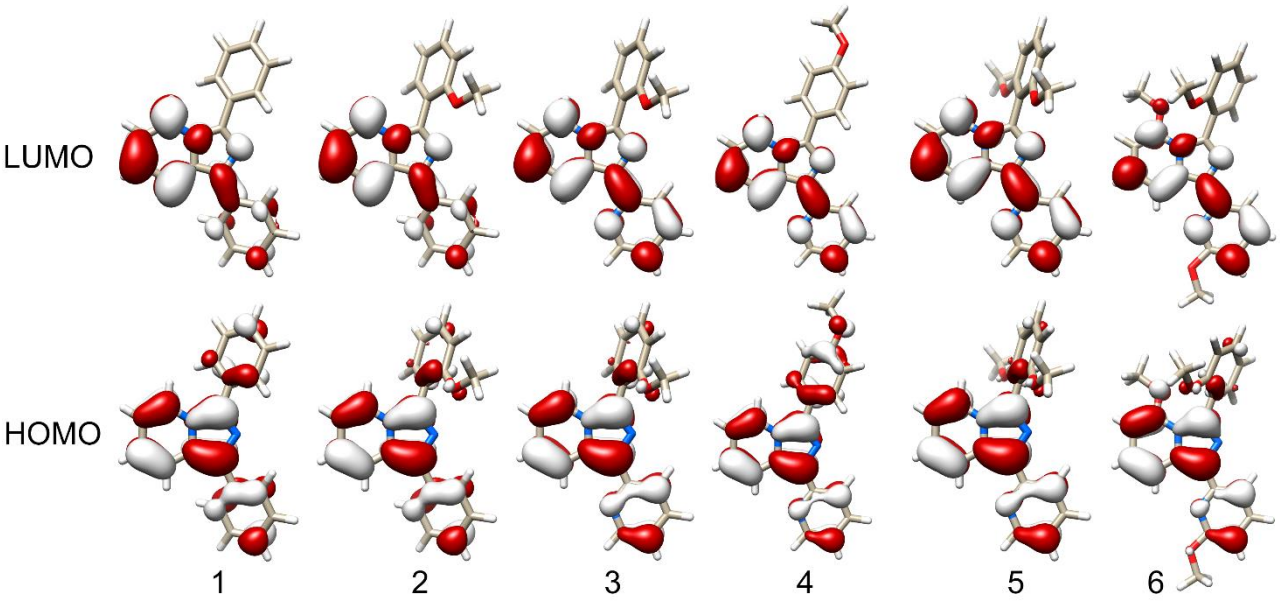

Figure 4. DFT calculated frontier molecular orbitals of **1**–**6**.

Table 2. Redox potentials (vs. ferrocenium/ferrocene reference) of **1**–**6** in dichloromethane solution (5 mM) together with DFT calculated energy of frontier molecular orbitals.

Compound	**Electrochemistry**			**DFT**	
	E^{OX}_{onset} **(V)**	$E_{1/2}^{ox}$ **(V)**	E_{HOMO} **(eV)**	E_{HOMO} **(eV)**	E_{LUMO} **(eV)**
1	0.409	0.482	-5.17	-5.06	-1.16
2	0.355	0.435	-5.10	-5.03	-1.11
3	0.389	0.438	-5.14	-5.10	-1.25
4	0.344	0.422	-5.08	-5.02	-1.28
5	0.348	0.417	-5.09	-5.07	-1.20
6	0.079	0.128	-4.71	-4.93	-1.10

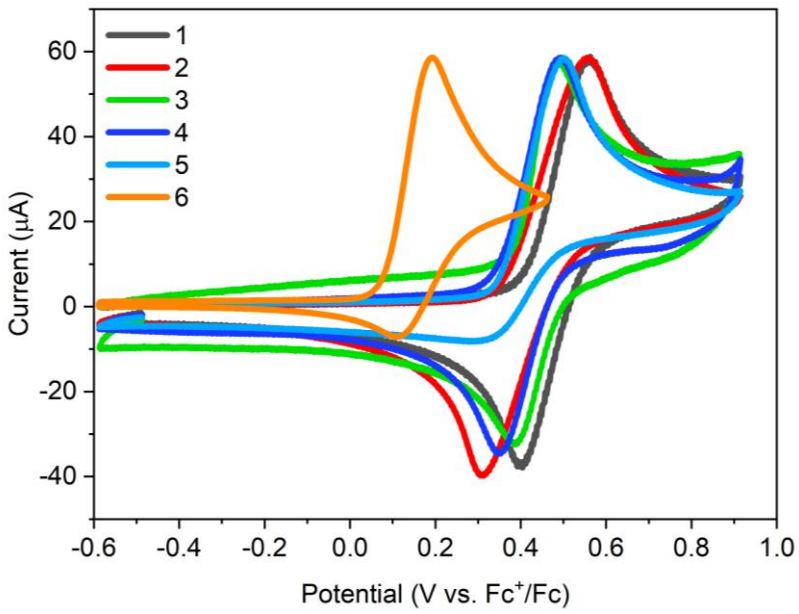

Figure 5. Normalized cyclic voltammetry: oxidation process of **1**–**6** in dichloromethane solution (5 mM).

Electrochemical properties of a new fluorophore are of paramount importance, in view of possible applications. For example, the absolute energy-level position of frontier orbital is a fundamental

information for the choice of electro-active materials, to effectively inject charge carriers into thin films of organic molecules or act as hole transporting materials. Table 2 and Figure 5 summarize the oxidation process of **1**–**6**, analysed by cyclic voltammetry in dichloromethane solution. The six compounds display a monoelectronic oxidation, characterized by half-wave potential $E_{1/2}$ of about 400 mV (versus ferrocene/ferrocenium reference, Fc/Fc^{+}), as previously reported for imidazo[1,5-*a*]pyridine derivatives.[21,22,38–41] **1**–**4** show chemically reversible oxidation waves, while in the case of **5** and **6** they are quasi-reversible. Moreover, the trimethoxylated derivative **6** is oxidized at less-positive potential, attesting the significant electron-donating effect of the methoxy substituent directly bond on the imidazo[1,5-*a*]pyridine nucleus (less positive $E_{1/2}^{ox}$, E^{ox}_{onset}, and an increase in HOMO energy). The energy of the HOMO was estimated by cyclic voltammetry and compared whit the result of DFT calculations. The oxidation onset potential E^{ox}_{onset} was derived by cyclic voltammogram traces and converted according to its relationship to the ionization energy (E_i), as proposed by D'Andrade et al.:[42]

$$E_{HOMO} \approx -E_i \approx -(4.6\ eV + 1.4 \cdot E^{ox}_{onset})$$

The energies of the HOMO determined by electrochemistry match very well those calculated by DFT. In dichloromethane solution, all the imidazo[1,5-*a*]pyridines exhibit an intense emission in the blue region of the spectrum, as previously reported by us.[43–46] In detail, the intense fluorescence is centred at λ_{max}~ 450-480 nm, with ϕ values ranging from 22% to 50% (**1** and **5** respectively). These values are comparable to the best results previously reported in literature for imidazo[1,5-*a*]pyridine derivatives.[33,35,44,45,47–49] The emission maximum is strongly influenced by the chemical structure. Indeed, the synthetic strategies employed to design compounds **1**–**6** allow obtaining 50 nm of blue shift for the emission, going from **1** to **6** (Figure 6).

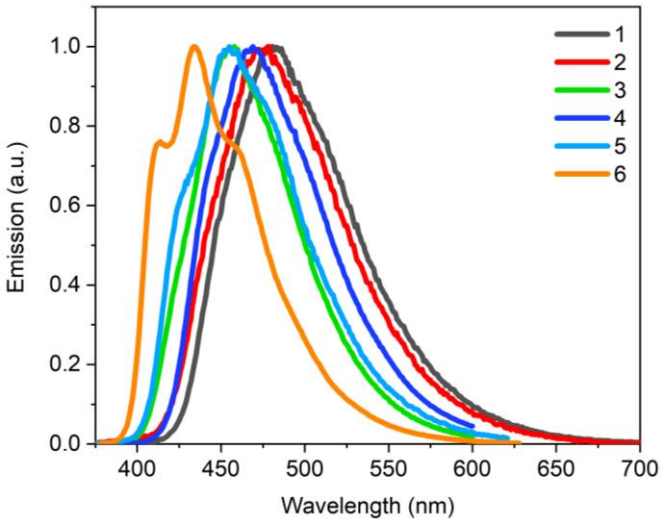

Figure 6. Normalized emission spectra of **1**–**6** in dichloromethane solution (10^{-5} M).

According to literature data, the introduction of the pendant pyridine group in position 1 on the imidazo[1,5-*a*]pyridine, compared to the introduction of *e.g.* a phenyl pendant group, could increase the ϕ values.[25,50,51] However, compounds **2** and **3** show comparable ϕ of 38% and 36%, respectively, indicating that the introduction of the pyridine is not particularly effective from this point of view. Nevertheless, the important presence of the pendant pyridine guarantees the typical bidentate ligand motif, which is well-known for allowing suitable complexation reactions and optoelectronic applications. [29,41,52–55] Moreover, the substitution of the benzene ring with a

pyridine in position 1 on the imidazo[1,5-*a*]pyridine causes a blue shift of the emission spectra of about 20 nm, as evidenced comparing **2** and **3**.

Besides the modification in position 1 on the imidazo[1,5-*a*]pyridine nucleus, we focused our attention on the introduction of electro-donating methoxy groups in different positions. This substituent is considered one of the more effective to increase the emissive behaviour of imidazo[1,5-*a*]pyridines.[32–35] Comparing the absorption and emission profiles of **1** and **2**, no significant differences are evidenced; however, the quantum yield doubles, suggesting the fundamental structural role of the methoxy in blocking the rotation of the phenyl substituent in position 3. The comparison between **3**, **4** and **5** emphasizes the importance of the substitution in position 3 on the imidazo[1,5-*a*]pyridines nucleus. The best results are obtained when the methoxy group is introduced in *ortho* on the phenyl pendant group (**3**, **5** and **6**). Indeed, the methoxy group in *para*, as for compound **4**, leads to a ϕ comparable to that of the unsubstituted compound **1**. This decrease can be attributed to the unlocking of the rotation in compound **4**. The hypothesis is further supported by the excellent results obtained by introducing two methoxy substituents in *ortho* (**5**). Indeed, in this case a large Stokes shift and the highest quantum yield among all the compounds considered are successfully achieved (ϕ enhanced up to 50%). Finally, compound **6** shows three methoxy groups: one on the imidazo[1,5-*a*]pyridine nucleus and two on the pendant (phenyl and pyridine) substituents. Compound **6** shows the strongest blue shift and an intermediate quantum yield (36%), comparable to other mono-*ortho* substituted compounds **2** and **3**.

The analysis of rotational energy barriers, calculated using DFT for the phenyl substitute in position 3, supports this interpretation (Figure 7). Compounds **1** and **4** have the lower emission quantum yield, the methoxy group is absent or is in *para* position, the rotational energy barrier (67 kJ mol^{-1}) is lower than the thermal energy available for molecules at room temperature and the free internal rotation favours non-radiative transition back to the ground state. In compounds **2** and **3** the barriers are higher (100 kJ mol^{-1} for synperiplanar and 750 kJ mol^{-1} for antiperiplanar conformations), the steric hindrance of the methoxy group in *ortho* position avoids the complete rotation, increasing the emission quantum yield. Finally, in compounds **5** and **6**, the two methoxy substituents in *ortho* position (**5**) and the steric interaction of the two overlapping methoxy groups (**6**) completely preclude the rotation of the phenyl ring (both energy barriers greatly exceed the critical threshold of 100 kJ mol^{-1}). In **5**, this results in a marked increase of the emission quantum yield up to 50%. In the case of **6**, despite the rotation blocking, the quantum yield does outperform the results of **2** and **3**, suggesting the existence of alternative deactivation pathways, established with the introduction of three methoxy groups.

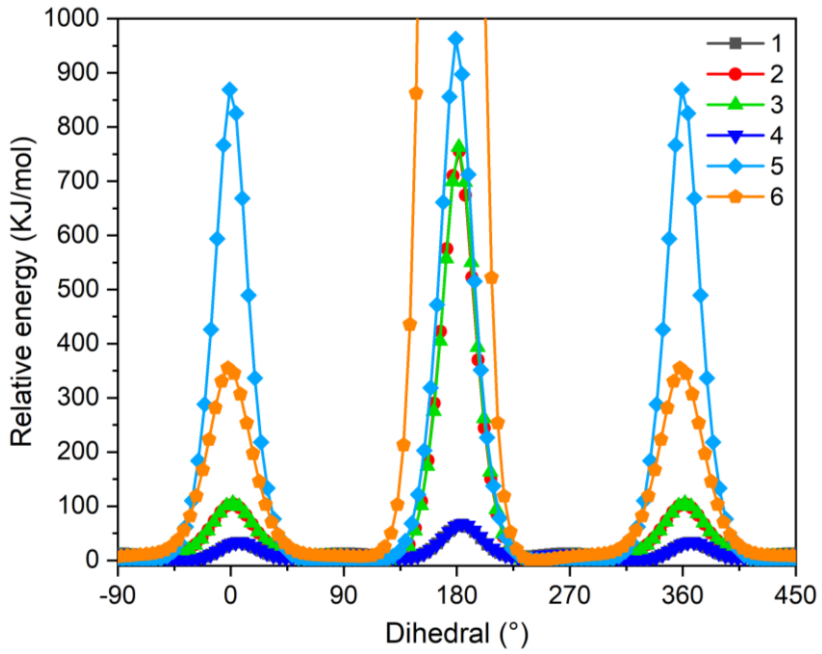

Figure 7. Rotational barrier energy profile calculated for the rotation of the phenyl substituent in position 3 on the imidazo[1,5-*a*]pyridine skeleton of **1**–**6**.

According to these observations, the reported structural modifications have different and definite effects on the optical properties. The substitution of the benzene ring with a pyridine in position 1 on the imidazo[1,5-*a*]pyridine causes a blue shift of the emission spectra of about 20 nm (as evidenced comparing **2** and **3**). The electronic role of the methoxy substituent is modest but evident, as demonstrated by the marked blue shift obtained for **6**, introducing three methoxy substituents. Even more noteworthy is the structural role of the methoxy introduced in *ortho* (**2**, **3**, **4**, **6**), allowing to block the rotation of the phenyl ring with a marked increase of the emission quantum yield. In general, compound **5** represents the best candidate for optical application because of its intense emission with great quantum yield and large Stokes shift. A preliminary test of the photostability of these compounds, performed by multiple emission experiments in dichloromethane solution (see Figure S1 in supplementary data section for **2** and **5**), reveals good medium-term stability (3.5% degradation after 3 hours), compatible with the use of these compounds as free emitters in sensors or fluorescence microscopy imaging.

3. Experimental details

3.1 Materials and techniques

All solvents and raw materials were used as received from commercial suppliers (Sigma-Aldrich and Alfa Aesar) without further purification.

TLC was performed on Fluka silica gel TLC-PET foils GF 254, particle size 25 nm, medium pore diameter 60 Å. Column chromatography was performed on Sigma-Aldrich silica gel 60 (70-230 mesh ASTM).

Elemental composition was determined using a Thermo FlashEA 1112 Series elemental analyser. Three replicas were performed and values were presented as % mass mean value.

^{1}H and ^{13}C NMR spectra were recorded on a JEOL ECP 400 FT-NMR spectrometer (^{1}H NMR operating frequency 400 MHz). Chemical shifts are reported relative to TMS ($\delta = 0$) and referenced

against solvent residual peaks. The following abbreviations are used: s (singlet), d (doublet), t (triplet), dd (doublet of doublets), m (multiplet).
Mass spectra were recorded on a Thermo-Finnigan Advantage Max Ion Trap Spectrometer equipped with an electrospray ion source (ESI) in positive and negative ion acquiring mode.
UV-Vis absorption spectra were recorded on a Cary60 spectrometer. Photoemission spectra, luminescence lifetimes and quantum yields were acquired with a HORIBA Jobin Yvon IBH Fluorolog-TCSPC spectrofluorometer, equipped with a Quanta-φ integrating sphere. The spectral response was corrected for the spectral sensitivity of the photomultiplier.
Cyclic voltammetry experiments were performed using a Metrohm Autolab 302 N potentiostat. The electrochemical cell was a single-compartment cell equipped with a standard three-electrode set-up: a glassy carbon working electrode (Ø = 1 mm), a Pt-wire counter electrode and a Ag/AgCl (KCl 3 M) reference electrode. All measurements were carried out in dichloromethane solution (5 mM) with tetrabutylammonium hexafluorophosphate (0.1 M) as supporting electrolyte.
All calculations were performed with the Gaussian 16 program package,[56] employing the Density Functional Theory (DFT) and its Time-Dependent extension TD-DFT.[57,58] The Becke three-parameter hybrid functional,[59] and the Lee− Yang – Parr's gradient corrected correlation functional (B3LYP)[60] were used together with the 6-31G** basis set.[61] The solvent effect was included using the polarizable continuum model (CPCM method),[62,63] with acetonitrile as solvent. Geometry optimizations were carried out for ground states, without any symmetry constraints. The nature of all stationary points was verified via harmonic vibrational frequency calculations, no imaginary frequencies were found, indicating we had located minima on potential energy surfaces. Rotational energy barriers were computed performing rigid potential energy surface scans (rotation of a dihedral angle between the imidazo[1,5-*a*]pyridine core and the phenyl substitute in position 3), and setting to zero the energy of the ground state optimized geometries. Electronic transitions were computed from the ground state, as vertical excitation with linear response solvation by TD-DFT,[57,58] employing the ground state optimized geometries. A total of 128 singlet excited states was computed for each compound, the electronic distribution and the localization of the singlet excited states were visualized using Electron Density Difference Maps. GaussSum 2.2.5[64] was used to simulate the theoretical UV-Vis spectra and for EDDMs calculations.[65,66] Molecular-graphic images were produced by using the UCSF Chimera package from the Resource for Biocomputing, Visualization, and Informatics at the University of California, San Francisco.[67]

3.2 Syntheses

Compounds **1**–**4** were prepared as previously reported: **1** and **2** [32,68–70], **3** [24], **4** [37,71]; compound **5** was prepared using a previously reported synthetic approach involving 2,6-dimethoxybenzoic acid, di(pyridin-2-yl)methanamine and propylphosphonic anhydride,[51,72] compound **6** has been prepared with a slight modification of a previously reported procedure.[23]

3-(2,6-dimethoxyphenyl)-1-(pyridin-2-yl)H-imidazo[1,5-*a*]pyridine (**5**).
2,6-dimethoxybenzoic acid (2.0 mmol, 364 mg) was added to a solution of di(pyridin-2-yl)methanamine (2.0 mmol, 370 mg), in *n*-butyl acetate (25 mL) at rt. The resulting slurry was added with 7.5 mL of T3P (propylphosphonic anhydride 50% solution in ethyl-acetate), the solution was stirred at room temperature for 1 h, before being heated at reflux for 16 h. The reaction mixture was cooled to room temperature and the *n*-butyl acetate was removed by evaporation under vacuum. The solid was dissolved in saturated sodium carbonate solution and the mixture extracted with CH_2Cl_2 (3

× 10 mL). The organic layer was separated, dried and the solvent evaporated under vacuum. The formed solid was washed several times with diethyl ether and dried under vacuum obtaining the product as a yellow powder (yield: 558 mg, 84%), melting point 178 °C. ^{1}H NMR (400 MHz, $CDCl_3$) δ 8.67 (d, J = 9.2 Hz, 1H), 8.61 (d, J = 4.8 Hz, 1H), 8.25 (d, J = 8.1 Hz, 1H), 7.67 (td, J = 7.7, 1.8 Hz, 1H), 7.42-7.46 (m, 2H), 7.05 (dd, J = 7.3, 4.8 Hz, 1H), 6.91 (dd, J = 9.2, 6.4 Hz, 1H), 6.69 (d, J = 8.5 Hz, 2H), 6.55 (t, J = 6.8 Hz, 1H), 3.73 (s, 6H). ^{13}C NMR (100 MHz, $CDCl_3$) δ 160.21, 155.61, 148.96, 136.13, 132.19, 131.93, 130.10, 129.66, 122.56, 121.42, 120.88, 120.23, 120.11, 112.82, 107.09, 104.25, 77.16, 56.13 MS (ESI) *m/z* calculated for $C_{20}H_{18}N_3O_2$ ($[M+H]^+$) 332.16; found 332.20. $C_{20}H_{17}N_3O_2$ requires C, 72.5; H, 5.2; N, 12.7%; found: C, 72.1; H, 5.3; N, 12.5%.

5-methoxy-3-(2-methoxyphenyl)-1-(6-methoxypyridin-2-yl)H-imidazo[1,5-*a*]pyridine (**6**).
A mixture consisting of bis(6-methoxypyridin-2-yl)methanone (2.00 mmol, 488 mg), 2-methoxybenzaldehyde (2.00 mmol, 272 mg), and ammonium acetate (10.00 mmol) in 25 mL of glacial acetic acid was stirred at 118 °C. After 12 h, the reaction mixture was cooled to room temperature and the acetic acid was removed by evaporation under vacuum. The solid was dissolved in an aqueous solution of Na_2CO_3 and the mixture extracted with CH_2Cl_2. The organic layer was separated and the solvent evaporated under vacuum. The formed solid was washed several times with diethyl ether and dried under vacuum obtaining a quantitative yield of the product as a yellow powder (yield: 506.99 mg, 70%), melting point 169 °C. ^{1}H NMR (400 MHz, acetone-d6) δ 8.38 (d, J = 8 Hz, 1H), 7.51-7.62 (d, 2H), 7.36-7.45 (m, 2H), 6.99-7.07 (m, 3H), 6.55 (d, J = 6.47 Hz, 1H), 6.07 (d, J = 6.47, 1H), 4.06 (s, 3H), 3.70 (s, 3H), 3.68 (s, 3H). ^{13}C NMR (100 MHz, acetone-d6) δ 138.71, 131.78, 130.77, 123.98, 120.30, 113.62, 112.73, 110.81, 109.78, 89.67, 66.11, 57.72, 56.72, 55.71, 54.96, 53.66, 18.90, 15.60. MS (ESI): m/z calculated for $C_{21}H_{20}N_3O_3$ [$(M+H^+)$] 362.14; found 362.18. $C_{21}H_{19}N_3O_3$ requires C, 69.8; H, 5.3; N, 11.6%; found: C, 69.5; H, 5.4; N, 11.5%.

4. Conclusions

This series of fluorescent 1,3-substituted imidazo[1,5-*a*]pyridine derivatives was designed to increase the optical performances of this well-known luminescent heterocyclic nucleus. The imidazo[1,5-*a*]pyridine core was substituted in different positions with one or more methoxy groups, and in position 1 with phenyl or pyridine pendant groups, employing convenient and highly accessible synthetic approaches.
The discussed compounds are characterized by absorption maxima in the near-UV region and no significant absorption in the visible range (λ_{max} < 430 nm), with a respectable transparency. The intense emissions in the spectral range between 400 and 550 nm, with quantum yield up to 50%, are associated to large Stokes shifts from 60 to 175 nm.
Investigating, both experimentally and computationally, the optical properties of the six molecules we unravelled and rationalized the possible correlations between the chemical structure and the electronic behaviour of these fluorophores, highlighting the key role of the rotation of the substituent group in position 1 and 3 on the imidazo[1,5-*a*]pyridine skeleton in increasing the emission quantum yield and in influencing the frontier molecular orbitals. Indeed, the comparison of the optical properties along the series emphasizes the importance of the substitutions in position 1 and 3.
We can conclude that the introduction of methoxy groups in different positions, and the change of the pendant group in position 1 on the imidazo[1,5-*a*]pyridine skeleton, have a modest effect on the absorption and emission ranges. On the other hand, **2**, **3**, **5** and **6** show a strong increase (up to 50%) of the emission quantum yield with respect to **1** and **4** (~20%). In particular, it is evident how

fundamental is the role of the steric hindrance of the methoxy groups introduced in *ortho* positions (**2**, **3**, **4**, **6**), allowing to partially or completely block the rotation of the phenyl ring, with a marked increase of the emission quantum yield.
Despite the explanation for the remaining 50% of non-radiative decay at this stage could be speculative, we believe that limiting the rotation of the substituent in position 1 could be crucial. Similarly, the quantum yield of **6**, which is lower than what can be inferred from the PES scan profile, suggests the existence of alternative deactivation pathways, established with the introduction of the three methoxy groups.
Moreover, different roles could be designed for this series of compounds. The practically null absorbance (very little for **5** and **6**) in the visible region, the relatively good quantum yield coupled with a large Stokes shift and an interesting photostability make them suitable for application as down-shifters for building integrated photovoltaic devices (e.g. smart window, greenhouse roofs, *etc*.). However, due to the reversible chemistry, they could be further employed as standing alone (or embedded in metal complexes) redox mediators for liquid or quasi-solid photovoltaic cells (e.g. DSSCs). In view of these possible applications, further studies are therefore needed, especially to verify the stability or their photo and electrochemical properties in environmental conditions.
In conclusion, this work gives a clear insight for the design of new derivatives towards application in fluorescence microscopy, down-converting technologies, lighting devices and other technological fields.

Acknowledgements

This project has received funding from the European Union's Horizon 2020 research and innovation program under grant agreement no. 826013 (IMPRESSIVE). CB and GV gratefully acknowledge research funding from the PON project "Tecnologia per celle solari bifacciali ad alta Efficienza a 4 terminali per utility scale" (BEST-4U), of the Italian Ministry MIUR (CUP B88D19000160005)". EC gratefully acknowledges research funding from the project number LTI19008 "National contact centre for non-exhaust traffic emissions" within the Programme INTER INFORM financed by the Ministry of Education, Youth and Sports of Czech Republic.

References

[1] Duan L, Hou L, Lee T-W, Qiao J, Zhang D, Dong G, et al. Solution processable small molecules for organic light-emitting diodes. J Mater Chem 2010;20:6392–407. https://doi.org/10.1039/B926348A.
[2] Fresta E, Costa RD. Beyond traditional light-emitting electrochemical cells – a review of new device designs and emitters. J Mater Chem C 2017;5:5643–75. https://doi.org/10.1039/C7TC00202E.
[3] Huang T, Jiang W, Duan L. Recent progress in solution processable TADF materials for organic light-emitting diodes. J Mater Chem C 2018;6:5577–96. https://doi.org/10.1039/C8TC01139G.
[4] Niko Y, Konishi G. Molecular Design of Highly Fluorescent Dyes. J Synth Org Chem Jpn 2012;70:918–27. https://doi.org/10.5059/yukigoseikyokaishi.70.918.
[5] Wei Q, Fei N, Islam A, Lei T, Hong L, Peng R, et al. Small-Molecule Emitters with High Quantum Efficiency: Mechanisms, Structures, and Applications in OLED Devices. Adv Opt Mater 2018;6:1800512. https://doi.org/10.1002/adom.201800512.
[6] Hong Y, Lam JWY, Tang BZ. Aggregation-induced emission: phenomenon, mechanism and applications. Chem Commun 2009:4332. https://doi.org/10.1039/b904665h.
[7] He S, Song J, Qu J, Cheng Z. Crucial breakthrough of second near-infrared biological window fluorophores: design and synthesis toward multimodal imaging and theranostics. Chem Soc Rev 2018;47:4258–78. https://doi.org/10.1039/C8CS00234G.

[8] Sedgwick AC, Wu L, Han H-H, Bull SD, He X-P, James TD, et al. Excited-state intramolecular proton-transfer (ESIPT) based fluorescence sensors and imaging agents. Chem Soc Rev 2018;47:8842–80. https://doi.org/10.1039/C8CS00185E.
[9] Alcarazo M, Roseblade SJ, Cowley AR, Fernandez R, Brown JM, Lassaletta JM. Imidazo[1,5-*a*]pyridine: A versatile architecture for stable N-heterocyclic carbenes. J Am Chem Soc 2005;127:3290–1. https://doi.org/10.1021/ja0423769.
[10] Song G-J, Bai S-Y, Dai X, Cao X-Q, Zhao B-X. A ratiometric lysosomal pH probe based on the imidazo[1,5-*a*]pyridine-rhodamine FRET and ICT system. Rsc Adv 2016;6:41317–22. https://doi.org/10.1039/c5ra25947a.
[11] Mohbiya DR, Sekar N. Tuning 'Stokes Shift' and ICT Character by Varying the Donor Group in Imidazo[1,5-*a*]pyridines: A Combined Optical, DFT, TD-DFT and NLO Approach. ChemistrySelect 2018;3:1635–44. https://doi.org/10.1002/slct.201702579.
[12] Volpi G, Lace B, Garino C, Priola E, Artuso E, Cerreia Vioglio P, et al. New substituted imidazo[1,5-*a*]pyridine and imidazo[5,1-a]isoquinoline derivatives and their application in fluorescence cell imaging. Dyes Pigments 2018;157:298–304. https://doi.org/10.1016/j.dyepig.2018.04.037.
[13] Yagishita F, Nii C, Tezuka Y, Tabata A, Nagamune H, Uemura N, et al. Fluorescent N-Heteroarenes Having Large Stokes Shift and Water Solubility Suitable for Bioimaging. Asian J Org Chem 2018;7:1614–9. https://doi.org/10.1002/ajoc.201800250.
[14] Hutt JT, Jo J, Olasz A, Chen C-H, Lee D, Aron ZD. Fluorescence Switching of Imidazo[1,5-*a*]pyridinium Ions: pH-Sensors with Dual Emission Pathways. Org Lett 2012;14:3162–5. https://doi.org/10.1021/ol3012524.
[15] Ge Y, Ji R, Shen S, Cao X, Li F. A ratiometric fluorescent probe for sensing Cu^{2+} based on new imidazo[1,5-*a*]pyridine fluorescent dye. Sens Actuators B Chem 2017;245:875–81. https://doi.org/10.1016/j.snb.2017.01.169.
[16] Wang L, Han X, Qu G, Su L, Zhao B, Miao J. A pH probe inhibits senescence in mesenchymal stem cells. Stem Cell Res Ther 2018;9:343. https://doi.org/10.1186/s13287-018-1081-0.
[17] Roy M, Chakravarthi BVSK, Jayabaskaran C, Karande AA, Chakravarty AR. Impact of metal binding on the antitumor activity and cellular imaging of a metal chelator cationic imidazopyridine derivative. Dalton Trans 2011;40:4855–64. https://doi.org/10.1039/c0dt01717e.
[18] Ingersoll MA, Lyons AS, Muniyan S, D'Cunha N, Robinson T, Hoelting K, et al. Novel Imidazopyridine Derivatives Possess Anti-Tumor Effect on Human Castration-Resistant Prostate Cancer Cells. PLOS ONE 2015;10:e0131811. https://doi.org/10.1371/journal.pone.0131811.
[19] Priyanga S, Khamrang T, Velusamy M, Karthi S, Ashokkumar B, Mayilmurugan R. Coordination geometry-induced optical imaging of L-cysteine in cancer cells using imidazopyridine-based copper(II) complexes. Dalton Trans 2019;48:1489–503. https://doi.org/10.1039/C8DT04634D.
[20] Ford NF, Browne LJ, Campbell T, Gemenden C, Goldstein R, Gude C, et al. Imidazo[1,5-*a*]Pyridines - a New Class of Thromboxane-A2 Synthetase Inhibitors. J Med Chem 1985;28:164–70.
[21] Albrecht G, Geis C, Herr JM, Ruhl J, Göttlich R, Schlettwein D. Electroluminescence and contact formation of 1-(pyridin-2-yl)-3-(quinolin-2-yl)imidazo[1,5-*a*]quinoline thin films. Org Electron 2019;65:321–6. https://doi.org/10.1016/j.orgel.2018.11.032.
[22] Albrecht G, Herr JM, Steinbach M, Yanagi H, Göttlich R, Schlettwein D. Synthesis, optical characterization and thin film preparation of 1-(pyridin-2-yl)-3-(quinolin-2-yl)imidazo[1,5-*a*]quinoline. Dyes Pigments 2018;158:334–41. https://doi.org/10.1016/j.dyepig.2018.05.056.
[23] Fresta E, Volpi G, Garino C, Barolo C, Costa RD. Contextualizing yellow light-emitting electrochemical cells based on a blue-emitting imidazo-pyridine emitter. Polyhedron 2018;140:129–37. https://doi.org/10.1016/j.poly.2017.11.048.
[24] Weber MD, Garino C, Volpi G, Casamassa E, Milanesio M, Barolo C, et al. Origin of a counterintuitive yellow light-emitting electrochemical cell based on a blue-emitting heteroleptic copper(I) complex. Dalton Trans 2016;45:8984–93. https://doi.org/10.1039/C6DT00970K.
[25] Volpi G, Garino C, Priola E, Magistris C, Chierotti MR, Barolo C. Halogenated imidazo[1,5-*a*]pyridines: chemical structure and optical properties of a promising luminescent scaffold. Dyes Pigments 2019;171:107713. https://doi.org/10.1016/j.dyepig.2019.107713.

[26] Marchesi A, Brenna S, Ardizzoia GA. Synthesis and emissive properties of a series of tetrahydro (imidazo[1,5-*a*]pyrid-3-yl)phenols: a new class of large Stokes shift organic dyes. Dyes Pigments 2019;161:457–63. https://doi.org/10.1016/j.dyepig.2018.09.069.
[27] Mandal A, Patel BK. Rationalization of weak interactions in two fluorescence active imidazo-[1,5-*a*]-pyridine derivatives: A combined experimental and computational study. J Mol Struct 2017;1147:735–46. https://doi.org/10.1016/j.molstruc.2017.07.08.
[28] Guckian AL, Doering M, Ciesielski M, Walter O, Hjelm J, O'Boyle NM, et al. Assessment of intercomponent interaction in phenylene bridged dinuclear ruthenium(II) and osmium(II) polypyridyl complexes. Dalton Trans 2004:3943–9.
[29] Ardizzoia GA, Brenna S, Durini S, Therrien B. Synthesis and characterization of luminescent zinc(II) complexes with a N,N-bidentate 1-pyridylimidazo[1,5-*a*]pyridine ligand. Polyhedron 2015;90:214–20. https://doi.org/10.1016/j.poly.2015.02.005.
[30] Cheng G, So GK-M, To W-P, Chen Y, Kwok C-C, Ma C, et al. Luminescent zinc(II) and copper(I) complexes for high-performance solution-processed monochromic and white organic light-emitting devices. Chem Sci 2015;6:4623–35. https://doi.org/10.1039/c4sc03161j.
[31] Blanco-Rodríguez AM, Kvapilova H, Sykora J, Towrie M, Nervi C, Volpi G, et al. Photophysics of Singlet and Triplet Intraligand Excited States in [$ReCl(CO)_3$(1-(2-pyridyl)-imidazo[1,5-*a*]pyridine)] Complexes. J Am Chem Soc 2014;136:5963–73. https://doi.org/10.1021/ja413098m.
[32] Volpi G, Magnano G, Benesperi I, Saccone D, Priola E, Gianotti V, et al. One pot synthesis of low cost emitters with large Stokes' shift. Dyes Pigments 2017;137:152–64. https://doi.org/10.1016/j.dyepig.2016.09.056.
[33] Shibahara F, Kitagawa A, Yamaguchi E, Murai T. Synthesis of 2-azaindolizines by using an iodine-mediated oxidative desulfurization promoted cyclization of N-2-pyridylmethyl thioamides and an investigation of their photophysical properties. Org Lett 2006;8:5621–4. https://doi.org/10.1021/ol0623623.
[34] Shibahara F, Yamaguchi E, Kitagawa A, Imai A, Murai T. Synthesis of 1,3-diarylated imidazo[1,5-*a*]pyridines with a combinatorial approach: metal-catalyzed cross-coupling reactions of 1-halo-3-arylimidazo[1,5-*a*]pyridines with arylmetal reagents. Tetrahedron 2009;65:5062–73. https://doi.org/10.1016/j.tet.2009.02.062.
[35] Yamaguchi E, Shibahara F, Murai T. 1-Alkynyl- and 1-Alkenyl-3-arylimidazo[1,5-*a*]pyridines: Synthesis, Photophysical Properties, and Observation of a Linear Correlation between the Fluorescent Wavelength and Hammett Substituent Constants. J Org Chem 2011;76:6146–58. https://doi.org/10.1021/jo200864x.
[36] Yamaguchi E, Shibahara F, Murai T. Direct Sequential C3 and C1 Arylation Reaction of Imidazo[1,5-*a*]pyridine Catalyzed by a 1,10-Phenanthroline-Palladium Complex. Chem Lett 2011;40:939–40.
[37] Hu Z, Hou J, Liu J, Yu W, Chang J. Synthesis of imidazo[1,5-*a*]pyridines *via* I_2 -mediated sp^3 C–H amination. Org Biomol Chem 2018;16:5653–60. https://doi.org/10.1039/C8OB01501E.
[38] Volpi G, Garino C, Salassa L, Fiedler J, Hardcastle KI, Gobetto R, et al. Cationic Heteroleptic Cyclometalated Iridium Complexes with 1-Pyridylimidazo[1,5-*a*]pyridine Ligands: Exploitation of an Efficient Intersystem Crossing. Chem- Eur J 2009;15:6415–27. https://doi.org/10.1002/chem.200801474.
[39] Salassa L, Garino C, Albertino A, Volpi G, Nervi C, Gobetto R, et al. Computational and spectroscopic studies of new rhenium(I) complexes containing pyridylimidazo[1,5-*a*]pyridine ligands: Charge transfer and dual emission by fine-tuning of excited states. Organometallics 2008;27:1427–35. https://doi.org/10.1021/om701175z.
[40] Albrecht G, Rössiger C, Herr JM, Locke H, Yanagi H, Göttlich R, et al. Optimization of the Substitution Pattern of 1,3-Disubstituted Imidazo[1,5-*a*]Pyridines and -Quinolines for Electro-Optical Applications. Phys Status Solidi B 2020;257:1900677. https://doi.org/10.1002/pssb.201900677.
[41] Garino C, Ruiu T, Salassa L, Albertino A, Volpi G, Nervi C, et al. Spectroscopic and computational study on new blue emitting $ReL(CO)_3Cl$ complexes containing pyridylimidazo[1,5-*a*]pyridine ligands. Eur J Inorg Chem 2008:3587–91. https://doi.org/10.1002/ejic.200800348.

[42] D'Andrade BW, Datta S, Forrest SR, Djurovich P, Polikarpov E, Thompson ME. Relationship between the ionization and oxidation potentials of molecular organic semiconductors. Org Electron 2005;6:11–20. https://doi.org/10.1016/j.orgel.2005.01.002.
[43] Bori J, Behera N, Mahata S, Manivannan V. Synthesis of Imidazo[5, 1-*a*]isoquinoline and Its 3-Substituted Analogues Including the Fluorescent 3-(1-Isoquinolinyl)imidazo[5,1-*a*]isoquinoline. ChemistrySelect 2017;2:11727–31. https://doi.org/10.1002/slct.201702420.
[44] Yagishita F, Kozai N, Nii C, Tezuka Y, Uemura N, Yoshida Y, et al. Synthesis of Dimeric Imidazo[1,5-*a*]pyridines and Their Photophysical Properties. ChemistrySelect 2017;2:10694–8. https://doi.org/10.1002/slct.201702277.
[45] Volpi G, Magistris C, Garino C. FLUO-SPICES: natural aldehydes extraction and one-pot reaction to prepare and characterize new interesting fluorophores. Educ Chem Eng 2018;24:1–6. https://doi.org/10.1016/j.ece.2018.06.002.
[46] Volpi G, Magistris C, Garino C. Natural aldehyde extraction and direct preparation of new blue light-emitting imidazo[1,5-*a*]pyridine fluorophores. Nat Prod Res 2017:1–8. https://doi.org/10.1080/14786419.2017.1410803.
[47] Shibahara F, Sugiura R, Yamaguchi E, Kitagawa A, Murai T. Synthesis of Fluorescent 1,3-Diarylated Imidazo[1,5-*a*]pyridines: Oxidative Condensation-Cyclization of Aryl-2-Pyridylmethylamines and Aldehydes with Elemental Sulfur as an Oxidant. J Org Chem 2009;74:3566–8.
[48] Tverdiy D, Chekanov M, Savitskiy P, Syniugin A, Yarmoliuk S, Fokin A. Efficient Preparation of Imidazo[1,5-*a*]pyridine-1-carboxylic Acids. Synthesis 2016;48:4269–77. https://doi.org/10.1055/s-0035-1561489.
[49] Chandrasekar S, Sangeetha S, Sekar G. Synthesis of 1,3-Disubstituted Imidazo[1,5-*a*]pyridines through Oxidative C-N Bond Formation from Aryl-2-pyridylmethanols and Their Fluorescent Study. ChemistrySelect 2019;4:5651–5. https://doi.org/10.1002/slct.201901440.
[50] Volpi G, Garino C, Conterosito E, Barolo C, Gobetto R, Viscardi G. Facile synthesis of novel blue light and large Stoke shift emitting tetradentate polyazines based on imidazo[1,5-*a*]pyridine. Dyes Pigments 2016;128:96–100. https://doi.org/10.1016/j.dyepig.2015.12.005.
[51] Volpi G, Garino C, Priola E, Diana E, Gobetto R, Buscaino R, et al. Facile synthesis of novel blue light and large Stoke shift emitting tetradentate polyazines based on imidazo[1,5-a]pyridine – Part 2. Dyes Pigments 2017;143:284–90. https://doi.org/10.1016/j.dyepig.2017.04.034.
[52] Durini S, Ardizzoia GA, Therrien B, Brenna S. Tuning the fluorescence emission in mononuclear heteroleptic trigonal silver(I) complexes. New J Chem 2017;41:3006–14. https://doi.org/10.1039/C6NJ04058F.
[53] Ardizzoia GA, Brenna S, Durini S, Therrien B, Veronelli M. Synthesis, Structure, and Photophysical Properties of Blue-Emitting Zinc(II) Complexes with 3-Aryl-Substituted 1-Pyridylimidazo[1,5-*a*]pyridine Ligands: Blue-Emitting Zinc(II) Complexes. Eur J Inorg Chem 2014;2014:4310–9. https://doi.org/10.1002/ejic.201402415.
[54] Wei Q, Wei M-J, Ou Y-J, Zhang J-Y, Huang X, Cai Y-P, et al. Formation and conversion of six temperature-dependent fluorescent Zn^{II} -complexes containing two in situ formed N-rich heterocyclic ligands. RSC Adv 2017;7:6994–7002. https://doi.org/10.1039/C6RA25678C.
[55] Álvarez CM, Álvarez-Miguel L, García-Rodríguez R, Martín-Álvarez JM, Miguel D. 3-(Pyridin-2-yl)imidazo[1,5-*a*]pyridine (Pyridylindolizine) as Ligand in Complexes of Transition and Main-Group Metals: *N* , *N* -Chelating Ligands. Eur J Inorg Chem 2015;2015:4921–34. https://doi.org/10.1002/ejic.201500776.
[56] Frisch MJ, Trucks GW, Schlegel HB, Scuseria GE, Robb MA, Cheeseman JR, et al. Gaussian 16. Wallingford, CT: Gaussian, Inc.; 2016.
[57] Stratmann RE, Scuseria GE, Frisch MJ. An efficient implementation of time-dependent density-functional theory for the calculation of excitation energies of large molecules. J Chem Phys 1998;109:8218–24. https://doi.org/10.1063/1.477483.
[58] Casida ME, Jamorski C, Casida KC, Salahub DR. Molecular excitation energies to high-lying bound states from time-dependent density-functional response theory: Characterization and correction of the time-dependent local density approximation ionization threshold. J Chem Phys 1998;108:4439–49. https://doi.org/10.1063/1.475855.

[59] Becke AD. Density-functional thermochemistry. III. The role of exact exchange. J Chem Phys 1993;98:5648–52. https://doi.org/10.1063/1.464913.
[60] Lee CT, Yang WT, Parr RG. Development of the Colle-Salvetti Correlation-Energy Formula into a Functional of the Electron-Density. Phys Rev B 1988;37:785–9. https://doi.org/10.1103/PhysRevB.37.785.
[61] McLean AD, Chandler GS. Contracted Gaussian basis sets for molecular calculations. I. Second row atoms, Z=11–18. J Chem Phys 1980;72:5639–48. https://doi.org/10.1063/1.438980.
[62] Cossi M, Scalmani G, Rega N, Barone V. New developments in the polarizable continuum model for quantum mechanical and classical calculations on molecules in solution. J Chem Phys 2002;117:43–54. https://doi.org/10.1063/1.1480445.
[63] Miertus S, Scrocco E, Tomasi J. Electrostatic interaction of a solute with a continuum. A direct utilizaion of AB initio molecular potentials for the prevision of solvent effects. Chem Phys 1981;55:117–29.
[64] O'boyle NM, Tenderholt AL, Langner KM. cclib: A library for package-independent computational chemistry algorithms. J Comput Chem 2008;29:839–45. https://doi.org/10.1002/jcc.20823.
[65] Browne WR, O'Boyle NM, McGarvey JJ, Vos JG. Elucidating excited state electronic structure and intercomponent interactions in multicomponent and supramolecular systems. Chem Soc Rev 2005;34:641–63. https://doi.org/10.1039/B400513A.
[66] Headgordon M, Grana AM, Maurice D, White CA. Analysis of Electronic-Transitions as the Difference of Electron-Attachment and Detachment Densities. J Phys Chem 1995;99:14261–70. https://doi.org/10.1021/j100039a012.
[67] Pettersen EF, Goddard TD, Huang CC, Couch GS, Greenblatt DM, Meng EC, et al. UCSF Chimera-a visualization system for exploratory research and analysis. J Comput Chem 2004;25:1605–12. https://doi.org/10.1002/jcc.20084.
[68] Herr JM, Rössiger C, Albrecht G, Yanagi H, Göttlich R. Solvent-free microwave-assisted synthesis of imidazo[1,5-*a*]pyridine and –quinoline derivatives. Synth Commun 2019:1–10. https://doi.org/10.1080/00397911.2019.1650188.
[69] Wang J, Dyers L, Mason R, Amoyaw P, Bu XR. Highly efficient and direct heterocyclization of dipyridyl ketone to N,N-bidentate ligands. J Org Chem 2005;70:2353–6. https://doi.org/10.1021/jo047853k.
[70] Wang J, Mason R, VanDerveer D, Feng K, Bu XR. Convenient Preparation of a Novel Class of Imidazo[1,5-*a*]pyridines: Decisive Role by Ammonium Acetate in Chemoselectivity. J Org Chem 2003;68:5415–8. https://doi.org/10.1021/jo0342020.
[71] Siddiqui SA, Potewar TM, Lahoti RJ, Srinivasan KV. Ionic liquid promoted facile one-pot synthesis of 1-pyridylimidazo[1,5-*a*]pyridines from dipyridylketone and aryl aldehydes. Synth-Stuttg 2006:2849–54.
[72] Crawforth JM, Paoletti M. A one-pot synthesis of imidazo[1,5-*a*]pyridines. Tetrahedron Lett 2009;50:4916–8. https://doi.org/10.1016/j.tetlet.2009.06.061.